East Asian Journal on Applied Mathematics
doi: 10.4208/eajam.2025-065.211025

Vol. **xx**, No. x, pp. 1-19
xxx 2026

A New Hybrid Trigonometric WENO Scheme for Hamilton-Jacobi Equations

Liang Li[1], Zhengwei Hou[2], Liuyong Pang[1] and Jun Zhu[3,*]

[1]*School of Mathematics and Statistics, Huang Huai University, Zhumadian 463000, P.R. China.*
[2]*School of Mining Engineering, Heilongjiang University of Science and Technology, Harbin 150022, P.R. China.*
[3]*State Key Laboratory of Mechanics and Control of Mechanical Structures, Nanjing University of Aeronautics and Astronautics, Nanjing 210016, P.R. China.*

Received 28 March 2025; Accepted (in revised version) 21 October 2025.

Abstract. In this paper, we introduce a new hybrid weighted essentially non-oscillatory (WENO) scheme grounded in trigonometric polynomials for the solution of Hamilton-Jacobi equations. This innovative approach utilizes trigonometric polynomial reconstruction as an alternative to the conventional algebraic polynomial reconstruction. Notably, the proposed scheme demonstrates reduced truncation errors in smooth regions and enhanced resolution in nonsmooth regions, outperforming the classical trigonometric WENO scheme — cf. [J. Zhu and J.X. Qiu, *Commun. Comput. Phys.* **8** (2010)]. In particular, we have designed a novel streamlined hybrid strategy aimed at improving the computational efficiency of the scheme, which surpasses the classical WENO scheme in this regard. A comprehensive suite of numerical experiments has been undertaken to demonstrate the merits of the proposed scheme.

AMS subject classifications: 65M06, 35L99

Key words: WENO scheme, Hamilton-Jacobi equation, finite difference scheme, hybrid scheme.

1. Introduction

In this paper, our primary focus is on developing high-order numerical approximations for the Hamilton-Jacobi (HJ) equations

$$\psi_t + H(x_1, \ldots, x_n, t, \psi, \nabla\psi) = 0, \quad (x_1, \ldots, x_n) \in \Omega, \tag{1.1}$$

where H is the Hamiltonian function. This equation holds a paramount significance and occupies a pivotal position in numerous fields, including seismic wave propagation, geometric

*Corresponding author. *Email addresses:* liliangnuaa@163.com (L. Li), houzhengweiusth@163.com (Z. Hou), pangliuyong@163.com (L. Pang), zhujun@nuaa.edu.cn (J. Zhu)

optics, and optimal control. Despite the smoothness of the initial conditions and the Hamiltonian, Eqs. (1.1) often have no classical solution or the solution is not unique. To tackle the issue of well-posedness, Crandall *et al.* [11–13] laid the groundwork for the entropy conditions and viscous solutions, clarifying their properties and constructing a first-order monotone scheme [14]. Building on this, further research emerged. Recognizing issues with accuracy and dissipation in the monotone approach, Osher and Sethian [31] introduced advanced, higher-order upwind schemes. This advancement paved the way for the modification of a multitude of numerical schemes originally designed for solving hyperbolic conservation laws, enabling them to address HJ equations as well.

The ENO methods [35,36] effectively addressed numerical oscillations in problems with discontinuities. Harten *et al.* [17, 18] and Shu [34] tailored these high-order methods to HJ equations, resulting in the production of monotone fluxes [32]. Subsequently, Lafon and Osher [23] extended the methods to unstructured grids. In addition, weighted ENO schemes have been also used in [21,29]. Later on, Jiang and Peng [20] introduced a WENO-JP scheme, followed by central [5], Hermite [33], mapped [6], and unequal-sized WENO schemes [41] for structured meshes. At the same time, alternative numerical methods [8, 15, 16, 28, 30], including finite element methods [1, 4, 19, 24], have been developed.

In the real world, high-frequency oscillating phenomena are widespread and pose significant challenges for accurate simulation. It is worth mentioning that numerical methods based on trigonometric polynomial functions offer a superior approach to capturing these complexities. Trigonometric interpolation, first explored by Baron [3], laid the groundwork for the development of more advanced numerical schemes. Building on this foundation, trigonometric polynomials have been successfully incorporated into both ENO [9] and WENO [40] frameworks. These methods turned out to be very efficient in simulating high-frequency phenomena. Wang and Zhang [37–39] further refined the trigonometric weighted essentially non-oscillatory (TWENO) framework by introducing concept of non-uniform stencils. This led to the creation of the US-TWENO scheme [37], MR-TWENO scheme [38], and MUS-TWENO scheme [39], each offering unique advantages in capturing high-frequency oscillations. While these advanced schemes provide remarkable accuracy, their inherent nonlinearity can diminish computational efficiency. Therefore, ongoing research continues to explore ways to optimize these methods, striking a balance between accuracy and performance.

Zhu and Qiu [40] applied a TWENO scheme to Hamilton-Jacobi equation, devising a comprehensive framework tailored specifically for this purpose. They adopted the same stencil as in the WENO-JP scheme [20] and reconstructed the numerical flux using trigonometric polynomials. However, numerical results show that the TWENO scheme does not exhibit exceptional performance in solving the Hamilton-Jacobi equations. To highlight its potential advantages, we develop a hybrid strategy, blending it with high-order trigonometric polynomials. A wide array of hybrid schemes exist for WENO schemes, encompassing approaches like TVB [10], KXRCF [22], etc. Li and Qiu [25–27] have thoroughly examined and studied various hybrid WENO schemes, totaling in dozens. Among the myriad hybrid schemes for the WENO scheme, the one proposed by Zhu [42] stands out due to its straightforward construction and practical ease of application, capturing widespread attention and

adoption. However, a pivotal step in this scheme involves identifying extreme points of high-order polynomials, which poses a formidable challenge when dealing with high-order trigonometric polynomials. To seamlessly integrate this hybrid approach into the TWENO scheme, modifications and enhancements are imperative.

In order to circumvent the complexity of determining the extreme points of high-order trigonometric polynomials, we dissect the high-order polynomial into three manageable low-order polynomials, subsequently identifying the hybrid strategy through the solution of the extreme points of these simplified polynomials. To further elevate the resolution of the hybrid TWENO scheme, we integrate not merely with a quartic trigonometric polynomial, but also with two cubic trigonometric polynomials. This innovative hybrid approach marks a substantial advancement. The comprehensive construction procedure of this scheme will be elaborated in the subsequent section.

This paper introduces a novel fifth-order finite difference scheme, specifically a hybrid trigonometric weighted essentially non-oscillatory (HTWENO) method, tailored for solving Hamilton-Jacobi equations on structured grids. The scheme boasts several key advantages. Firstly, it adopts a novel approach to spatial reconstruction, leveraging trigonometric polynomials as basis functions for the reconstruction process. Secondly, it introduces an innovative hybrid strategy, significantly enhancing the scheme's resolution and robustness. Lastly, it exhibits remarkable computational efficiency, offering notable improvements over traditional WENO schemes.

The structure of this paper is as follows. Section 2 elaborates on the comprehensive spatial construction methods employed in a hybrid trigonometric WENO scheme for Hamilton-Jacobi equations. In Section 3, we evaluate the efficacy of a novel finite difference hybrid trigonometric WENO scheme by using various benchmark examples. Finally, Section 4 contains concluding observations.

2. A WENO Finite Difference Method

In this section, we offer an exhaustive explanation of the construction methodology for the innovative finite difference hybrid trigonometric weighted essentially non-oscillatory approach tailored to solve the Hamilton-Jacobi equations. We commence by concentrating on the one-dimensional control equations (1.1). To ensure clarity and streamline the explanation, the computational domain Ω is partitioned into a uniform grid, where each interval I_i is defined as $[x_{i-1/2}, x_{i+1/2}]$ for i varying from 1 to N. Here, x_i represents the midpoint of the interval, calculated as $(x_{i-1/2} + x_{i+1/2})/2$, and $|I_i|$ denotes the length of I_i, specifically Δx. Subsequently, we reformulate the one-dimensional version of the Eq. (1.1) as

$$\psi_t + H(x, t, \psi, \psi_x) = 0, \quad \psi(x, 0) = \psi_0(x).$$

Introducing the notation $\psi_i \equiv \psi_i(t) = \psi(x_i, t)$, we define $\triangle^+\psi_i$ as $\psi_{i+1} - \psi_i$ and consider the following numerical approximation of the Hamiltonian H:

$$\frac{d\psi_i(t)}{dt} = L(\psi_i) = -\hat{H}\big(x_i, t, \psi_i, \psi^+_{x,i}, \psi^-_{x,i}\big). \tag{2.1}$$

In this context, $\hat{H}$ represents a Lipschitz continuous and monotone flux that is consistent with H such that

$$\hat{H}(x,t,\psi,\psi^+,\psi^-) = H\left(x,t,\psi,\frac{\psi^+ + \psi^-}{2}\right),$$

whenever $\psi^+ = \psi^-$. We employ the Lax-Friedrichs numerical flux — viz. the monotone numerical Hamiltonian

$$\hat{H}(x,t,\psi,\psi^+,\psi^-) = H\left(x,t,\psi,\frac{\psi^+ + \psi^-}{2}\right) - \alpha\frac{\psi^+ - \psi^-}{2},$$

where α is the maximum of the absolute value of $H'(\psi_x)$, with H' representing the partial derivative of H concerning ψ_x. In the semi-discrete formulation (2.1), $\psi^-_{x,i}$ and $\psi^+_{x,i}$ respectively denote the left and right approximations of $(\psi_x)_i$ at the point x_i. To clarify the spatial reconstruction process, we will focus on $\psi^-_{x,i}$ as an example. To demonstrate the advantages of our newly designed scheme, we conducted comparisons with the traditional WENO-JP scheme, WENO-Z scheme, and TWENO scheme. However, since the WENO-Z and TWENO schemes have not been previously used to solve the HJ equations, we also present their reconstruction processes below.

2.1. The WENO-Z reconstruction

Firstly, we do a WENO-Z type reconstruction. This reconstruction is based on classic WENO-JP reconstruction [7] and is obtained by adding global smoothness indicators to nonlinear weights. We choose the same set of equal-sized spatial stencils $T_1 = \{x_{i-3}, x_{i-2}, x_{i-1}, x_i\}$, $T_2 = \{x_{i-2}, x_{i-1}, x_i, x_{i+1}\}$, and $T_3 = \{x_{i-1}, x_i, x_{i+1}, x_{i+2}\}$ as in the WENO-JP reconstruction. Then we construct three quadratic polynomials such that

$$\frac{1}{\Delta x}\int_{x_m}^{x_{m+1}} p_k(x)dx = \frac{\Delta^+\psi_m}{\Delta x}, \quad m = i-4+k,\ldots,i-2+k, \quad k = 1,2,3.$$

From each spatial stencils T_k, we can individually derive a third-order approximation of $\psi^-_{x,i}$ on the left side of x_i

$$\begin{aligned}
\psi^{-,1}_{x,i} &= p_1(x_i) = \frac{2\Delta^+\psi_{i-3} - 7\Delta^+\psi_{i-2} + 11\Delta^+\psi_{i-1}}{6\Delta x},\\
\psi^{-,2}_{x,i} &= p_2(x_i) = \frac{-\Delta^+\psi_{i-2} + 5\Delta^+\psi_{i-1} + 2\Delta^+\psi_i}{6\Delta x},\\
\psi^{-,3}_{x,i} &= p_3(x_i) = \frac{2\Delta^+\psi_{i-1} + 5\Delta^+\psi_i + \Delta^+\psi_{i+1}}{6\Delta x}.
\end{aligned}$$

We employ the smoothness indicators β_k to assess the smoothness of the function $p_k(x)$ within the interval $[x_{i-1}, x_i]$. The principle for calculating it is similar to the one in [2,21]. The formula used in the calculation has the form

$$\beta_k = \sum_{\alpha=1}^{2}\int_{x_{i-1}}^{x_i} \Delta x^{2\alpha-1}\left(\frac{d^\alpha p_k(x)}{dx^\alpha}\right)^2 dx, \quad k = 1,2,3. \tag{2.2}$$

The nonlinear weights ω_k^Z are computed by a formula that incorporates predefined linear weights d_k and smoothness indicators β_k, viz.

$$\omega_k^Z = \frac{\overline{\omega}_k}{\sum_{m=1}^{3} \overline{\omega}_m},$$

where

$$\overline{\omega}_k = d_k\left(1 + \frac{|\beta_1 - \beta_3|}{\beta_k + 10^{-6}}\right), \quad k = 1,2,3.$$

The linear weights are specified as $d_1 = 1/10$, $d_2 = 6/10$, and $d_3 = 3/10$. The final WENO-Z type reconstruction is

$$\psi_{x,i}^{-} = \omega_1^Z \psi_{x,i}^{-,1} + \omega_2^Z \psi_{x,i}^{-,2} + \omega_3^Z \psi_{x,i}^{-,3}.$$

2.2. The TWENO reconstruction

This scheme utilizes identical spatial stencils as the one introduced in the preceding section, albeit with distinct bases employed for the reconstruction of the polynomial. Reconstructing three quadratic trigonometric polynomials $p_k(x)$ within the span$\{1, \sin(x - x_{i-1/2}), \cos(x - x_{i-1/2}) - \sin(\Delta x/2)/(\Delta x/2)\}$ on stencils T_k that fulfill the condition given by Eq. (2.3) is straightforward. The equation ensures that

$$\frac{1}{\Delta x}\int_{x_m}^{x_{m+1}} p_k(x)dx = \frac{\Delta^+ \psi_m}{\Delta x}, \quad m = i-4+k, \ldots, i-2+k, \quad k = 1,2,3. \tag{2.3}$$

This allows for accurate and efficient polynomial reconstruction. The explicit formulas for $p_k(x_i)$ are

$$\begin{aligned}
\psi_{x,i}^{-,1} = p_1(x_i) = {} & \frac{-\Delta x}{\sin(2\Delta x)(2+4\cos(\Delta x))} \\
& \times \Big(2\Delta^+\psi_{i-1} - 3\Delta^+\psi_i + (3\Delta^+\psi_{i-1} - \Delta^+\psi_{i-2} - 5\Delta^+\psi_i)\cos(\Delta x) \\
& \quad + (\Delta^+\psi_{i-1} - \Delta^+\psi_{i-2} - 3\Delta^+\psi_i)\cos(2\Delta x) + \Delta^+\psi_{i-1}\cos(3\Delta x)\Big), \\
\psi_{x,i}^{-,2} = p_2(x_i) = {} & \frac{\Delta x}{\sin(2\Delta x)(2+4\cos(\Delta x))} \\
& \times \Big(2\Delta^+\psi_i + \Delta^+\psi_{i+1} - (\Delta^+\psi_{i-1} - 2\Delta^+\psi_i - \Delta^+\psi_{i+1})\cos(\Delta x) \\
& \quad + (\Delta^+\psi_i \cos(2\Delta x)\Big), \\
\psi_{x,i}^{-,3} = p_3(x_i) = {} & \frac{\Delta x}{\sin(2\Delta x)(2+4\cos(\Delta x))} \\
& \times \Big(\Delta^+\psi_i + 2\Delta^+\psi_{i+1} + (\Delta^+\psi_i + 2\Delta^+\psi_{i+1} - \Delta^+\psi_{i+2})\cos(\Delta x) \\
& \quad + (\Delta^+\psi_{i+1}\cos(2\Delta x)\Big).
\end{aligned}$$

Subsequently, a quartic trigonometric polynomial $p^5(x) \in \text{span}\{1, \sin(x - x_{i-1/2}), \cos(x - x_{i-1/2}) - \sin(\Delta x/2)/(\Delta x/2), \sin(2(x - x_{i-1/2})), \cos(2(x - x_{i-1/2})) - \sin(\Delta x)/(\Delta x)\}$ such that

$$\frac{1}{\Delta x}\int_{x_m}^{x_{m+1}} p^5(x)dx = \frac{\Delta^+\psi_m}{\Delta x}, \quad m = i-3, i-2, i-1, i, i+1$$

is calculated to determine linear weights γ_k. More exactly, using the equation

$$p^5(x_i) = \gamma_1 p_1(x_i) + \gamma_2 p_2(x_i) + \gamma_3 p_3(x_i),$$

we get

$$\begin{aligned}
\gamma_1 &= \frac{1}{2 + 4\cos(\Delta x) + 2\cos(2\Delta x) + 2\cos(3\Delta x)},\\
\gamma_2 &= \frac{\cos(\Delta x) + \cos(2\Delta x) + \cos(3\Delta x)}{1 + 2\cos(\Delta x) + \cos(2\Delta x) + \cos(3\Delta x)},\\
\gamma_3 &= \frac{1 + 2\cos(\Delta x)}{2 + 4\cos(\Delta x) + 2\cos(2\Delta x) + 2\cos(3\Delta x)}.
\end{aligned} \tag{2.4}$$

Then, the smoothness indicators β_k can be computed employing formula (2.2). Integrating this with the weights (2.4), we determine nonlinear weights ω_k^T, viz.

$$\omega_k^T = \frac{\overline{\omega}_k}{\sum_{m=1}^3 \overline{\omega}_m}, \quad \overline{\omega}_k = \frac{\gamma_k}{(\beta_k + 10^{-6})^2}, \quad k = 1, 2, 3. \tag{2.5}$$

The final reconstruction has the form

$$\psi^-_{x,i} = \omega_1^T \psi^{-,1}_{x,i} + \omega_2^T \psi^{-,2}_{x,i} + \omega_3^T \psi^{-,3}_{x,i}.$$

Remark 2.1. The accuracy of the TWENO scheme has been studied in [40].

2.3. The HTWENO reconstruction

This approach improves TWENO schemes by direct application of a linear scheme in smooth regions and TWENO scheme in non-smooth ones. The main difference between this and traditional hybrid schemes consists in the hybridization of the TWENO scheme with three linear schemes simultaneously. This approach enables higher resolution in areas of discontinuity. The specific construction method is outlined as follows. Firstly, three spatial templates, T_1, T_2 and T_3, identical to those used in the TWENO scheme, are selected. We reconstruct quadratic trigonometric polynomials $p_1(x)$, $p_2(x)$, $p_3(x) \in \text{span}\{1, \sin(x - x_{i-1/2}), \cos(x - x_{i-1/2}) - \sin(\Delta x/2)/(\Delta x/2)\}$ and cubic trigonometric polynomials $p_1^4(x)$, $p_2^4(x) \in \text{span}\{1, \sin(x - x_{i-1/2}), \cos(x - x_{i-1/2}) - \sin(\Delta x/2)/(\Delta x/2), \sin(2(x - x_{i-1/2}))\}$ which satisfy

$$\begin{aligned}
&\frac{1}{\Delta x}\int_{x_m}^{x_{m+1}} p_k(x)dx = \frac{\Delta^+\psi_m}{\Delta x}, \quad m = i-4+k, \ldots, i-2+k, \quad k = 1, 2, 3,\\
&\frac{1}{\Delta x}\int_{x_m}^{x_{m+1}} p_k^4(x)dx = \frac{\Delta^+\psi_m}{\Delta x}, \quad m = i-4+k, \ldots, i-1+k, \quad k = 1, 2.
\end{aligned}$$

The polynomials $p_k(x)$ and $p_k^4(x)$ can be readily computed, and linear weights can be obtained from the following equations:

$$p_1^4(x_i) = \gamma_4 p_1(x_i) + \gamma_5 p_2(x_i), \quad p_2^4(x_i) = \gamma_6 p_2(x_i) + \gamma_7 p_3(x_i).$$

The coefficients γ_4, γ_5, γ_6, and γ_7 are linear weights. They have the form

$$\begin{aligned}
\gamma_4 &= \frac{\Delta x - \Delta x\cos(\Delta x)}{2\cos(\Delta x)(2\cos(\Delta x)+1)(\Delta x\cos(\Delta x)+\sin(\Delta x))},\\
\gamma_5 &= 1 - \frac{\Delta x - \Delta x\cos(\Delta x)}{2\cos(\Delta x)(2\cos(\Delta x)+1)(\Delta x\cos(\Delta x)+\sin(\Delta x))},\\
\gamma_6 &= \frac{\Delta x - \Delta x\cos(\Delta x)}{2\cos(\Delta x)(2\cos(\Delta x)+1)(\Delta x-\sin(\Delta x))},\\
\gamma_7 &= 1 - \frac{\Delta x - \Delta x\cos(\Delta x)}{2\cos(\Delta x)(2\cos(\Delta x)+1)(\Delta x-\sin(\Delta x))}.
\end{aligned}$$

To find extreme point of the function $p_m(x)$, we set the derivative $p_m'(x)$ to zero and arrive at the equation

$$b_m\cos(x - x_{i-1/2}) = c_m\sin(x - x_{i-1/2}).$$

The solution of this equation is

$$\text{Root}_m = x_{i-1/2} + \arctan\left(\frac{b_m}{c_m+\varepsilon}\right).$$

The solution incorporates a small parameter ε introduced to avoid zero denominator. In what follows, $\varepsilon = 10^{-10}$. We also note that three extreme points, referred to as $Root_m$, may not necessarily lie within their respective stencils T_m, i.e.

$$\frac{b_m}{c_m+\varepsilon} \notin \left[\left(\frac{2m-7}{2}\right)\Delta x, \left(\frac{2m-1}{2}\right)\Delta x\right], \quad m = 1,2,3.$$

To reconstruct the numerical flux $\psi_{x,i}^-$ at $x = x_i$, we employ the following linear approximation:

$$\psi_{x,i}^- = \gamma_1 p_1(x_i) + \gamma_2 p_2(x_i) + \gamma_3 p_3(x_i).$$

Besides, if $Root_1$ and $Root_2$ are outside of their respective stencils T_1 and T_2, but $Root_3$ is within T_3, then the flux is redefined as

$$\psi_{x,i}^- = \gamma_4 p_1(x_i) + \gamma_5 p_2(x_i).$$

Similarly, if $Root_2$ and $Root_3$ are exterior to T_2 and T_3, while $Root_1$ is interior to T_1, we set

$$\psi_{x,i}^- = \gamma_6 p_2(x_i) + \gamma_7 p_3(x_i).$$

If none of the extreme points satisfies all the conditions, linear approximation becomes infeasible for $\psi_{x,i}^-$. Instead, the following trigonometric weighted essentially non-oscillatory scheme should be adopted for reconstruction:

$$\psi_{x,i}^- = \omega_1^H p_1(x_i) + \omega_2^H p_2(x_i) + \omega_3^H p_3(x_i).$$

The nonlinear weights ω_k^H take the form

$$\omega_k^H = \frac{\bar{\omega}_k}{\sum_{l=1}^3 \bar{\omega}_l}, \quad \bar{\omega}_k = \gamma_k \left(1 + \frac{|\beta_1 - \beta_3|}{\beta_k + 10^{-6}}\right), \quad k = 1, 2, 3. \tag{2.6}$$

Smoothness indicators β_k and linear weights γ_k in Eq. (2.6) are identical to their counterparts in Eq. (2.5). We summarize the hybrid reconstruction procedure as follows.

Algorithm 2.1 Procedure for the Hybrid Reconstruction

Procedure HTWENO scheme
Give the values $\Delta^+\psi_m/(\Delta x)$ for all m.
Calculate $Root_1$, $Root_2$, $Root_3$ of the reconstruction polynomial for all stencil.
if $Root_1 \notin T_1$, $Root_2 \notin T_2$, $Root_3 \notin T_3$ **then**
  $\psi_{x,i}^- = \sum_{k=1}^3 \gamma_k p_k(x_i)$
else
  if $Root_1 \notin T_1$, $Root_2 \notin T_2$, $Root_3 \in T_3$ **then**
    $\psi_{x,i}^- = \gamma_4 p_1(x_i) + \gamma_5 p_2(x_i)$
  else
    if $Root_1 \in T_1$, $Root_2 \notin T_2$, $Root_3 \notin T_3$ **then**
      $\psi_{x,i}^- = \gamma_6 p_2(x_i) + \gamma_7 p_3(x_i)$
    else
      $\psi_{x,i}^- = \sum_{k=1}^3 \omega_k^H p_k(x_i)$.
    end if
  end if
end if

After applying different WENO reconstructions, we substitute $\psi_{x,i}^{\pm}$ into the Eq. (2.1) and obtain the ordinary differential equation

$$\frac{d\psi_i(t)}{dt} = L(\psi_i).$$

To solve this ODE, we can employ the total variation diminishing Runge-Kutta scheme — cf. [35]

$$\begin{aligned}
\psi^{(1)} &= \psi^n + \Delta t L(\psi^n), \\
\psi^{(2)} &= \frac{3}{4}\psi^n + \frac{1}{4}\psi^{(1)} + \frac{1}{4}\Delta t L\big(\psi^{(1)}\big), \\
\psi^{n+1} &= \frac{1}{3}\psi^n + \frac{2}{3}\psi^{(2)} + \frac{2}{3}\Delta t L\big(\psi^{(2)}\big).
\end{aligned}$$

For two-dimensional governing equations, computational approach is analogous to that in the one-dimensional case — cf. [20].

Remark 2.2. This hybrid scheme is defined by its use of linear weights in smooth regions, bypassing the need for computationally expensive nonlinear weights. This design offers multiple benefits and maintains the scheme order of accuracy. Consequently, the accuracy analysis matches that of the conventional TWENO scheme and is thus omitted.

3. Numerical Experiments

In this section, we evaluate the HTWENO scheme, affirming its outstanding performance by comparing it with WENO-JP, WENO-Z, and TWENO schemes.

Example 3.1 (One-Dimension Accuracy)**.** We test the accuracy of the new HTWENO scheme by considering the following one-dimensional linear equation:

$$\psi_t + \psi_x = 0, \quad (x,t) \in [-1,1] \times [0,2] \tag{3.1}$$

with the initial condition

$$\psi(x,0) = \sin\left(\pi x - \frac{\sin(\pi x)}{\pi}\right)$$

and periodic boundary conditions. The exact solution of the Eq. (3.1) is

$$\psi(x,t) = \sin\left(\pi(x-t) - \frac{\sin(\pi(x-t))}{\pi}\right).$$

Table 1 shows the errors and numerical accuracy associated with this solution. Note that the HTWENO scheme not only exhibits smaller truncation errors but also achieves higher computational efficiency. Fig. 1 clearly illustrates this point.

Table 1: Example 3.1. L_1 and L_∞ errors, orders and CPU time. HTWENO, TWENO, WENO-JP and WENO-Z schemes at $t = 2.0$.

	HTWENO				TWENO			
N	L_1 error	order	L_∞ error	order	L_1 error	order	L_∞ error	order
10	3.57E-02	–	6.68E-02	–	7.47E-02	–	1.98E-01	–
20	1.80E-03	4.31	4.96E-03	3.75	6.99E-03	3.42	1.49E-02	3.73
40	6.52E-05	4.79	1.77E-04	4.81	3.25E-04	4.43	8.39E-04	4.15
80	2.12E-06	4.94	5.99E-06	4.89	1.23E-05	4.72	3.25E-05	4.69
160	6.67E-08	4.99	1.88E-07	4.99	4.13E-07	4.90	1.02E-06	5.00
320	2.09E-09	5.00	5.89E-09	5.00	1.24E-08	5.06	2.88E-08	5.14
640	7.05E-11	4.89	2.21E-10	4.74	3.55E-10	5.13	9.34E-10	4.94
	WENO-JP				WENO-Z			
N	L_1 error	order	L_∞ error	order	L_1 error	order	L_∞ error	order
10	7.76E-02	–	2.06E-01	–	3.66E-02	–	6.67E-02	–
20	7.21E-03	3.43	1.58E-02	3.70	1.81E-03	4.33	5.01E-03	3.73
40	3.35E-04	4.43	8.78E-04	4.17	6.58E-05	4.78	1.80E-04	4.80
80	1.26E-05	4.73	3.22E-05	4.77	2.12E-06	4.95	5.99E-06	4.91
160	4.22E-07	4.90	1.01E-06	5.00	6.67E-08	4.99	1.88E-07	4.99
320	1.27E-08	5.06	3.01E-08	5.07	2.09E-09	5.00	5.89E-09	5.00
640	3.62E-10	5.13	9.48E-10	4.99	7.23E-11	4.99	2.10E-10	4.95

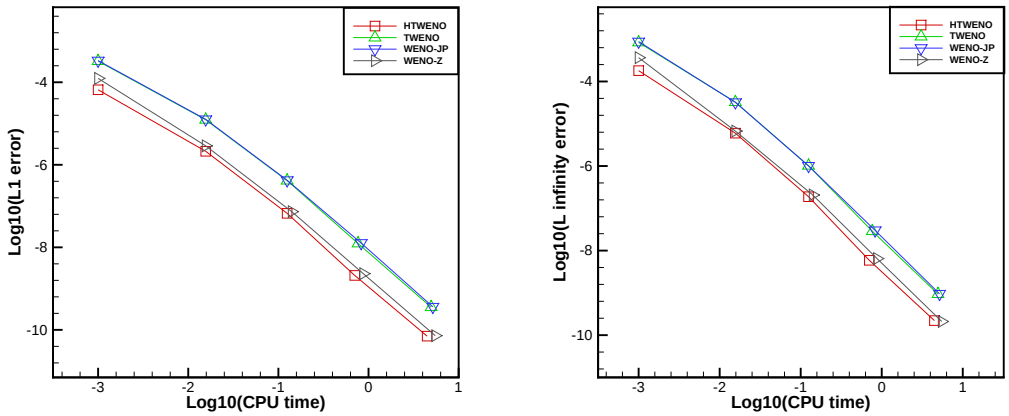

Figure 1: Example 3.1. Computing time and error.

Example 3.2 (Two-Dimension Accuracy Test)**.** Now we test the accuracy of the HTWENO scheme for the two-dimensional Burgers' equation

$$\psi_t + \frac{(\psi_x + \psi_y + 1)^2}{2} = 0, \quad (x, y) \in [-2, 2] \times [-2, 2] \tag{3.2}$$

with the initial condition

$$\psi(x, y, 0) = -\cos\left(\frac{\pi(x + y)}{2}\right)$$

and periodic boundary constraints. The computation terminates at $t = 0.5/\pi^2$, preserving solution smoothness throughout. Table 2 outlines L_1 and L_∞ errors, along with the nu-

Table 2: Example 3.2. L_1 and L_∞ errors, orders and CPU time. HTWENO, TWENO, WENO-JP and WENO-Z schemes at $t = 0.5/\pi^2$.

	HTWENO				TWENO			
$N \times N$	L_1 error	order	L_∞ error	order	L_1 error	order	L_∞ error	order
20 × 20	1.10E-04	–	4.83E-04	–	2.22E-04	–	1.44E-03	–
40 × 40	5.76E-06	4.25	6.29E-05	2.94	1.17E-05	4.24	1.38E-04	3.38
80 × 80	2.10E-07	4.78	2.57E-06	4.61	4.72E-07	4.64	5.95E-06	4.54
160 × 160	6.96E-09	4.91	8.85E-08	4.86	1.72E-08	4.78	2.03E-07	4.87
320 × 320	2.21E-10	4.97	2.83E-09	4.96	5.64E-10	4.93	6.48E-09	4.97
640 × 640	6.94E-12	5.00	8.91E-11	4.99	1.77E-11	4.99	2.05E-10	4.98
	WENO-JP				WENO-Z			
$N \times N$	L_1 error	order	L_∞ error	order	L_1 error	order	L_∞ error	order
20 × 20	2.70E-04	–	1.73E-03	–	1.18E-04	–	6.30E-04	–
40 × 40	1.36E-05	4.32	1.56E-04	3.48	6.01E-06	4.30	6.58E-05	3.26
80 × 80	5.31E-07	4.68	6.57E-06	4.57	2.22E-07	4.76	2.83E-06	4.54
160 × 160	1.90E-08	4.80	2.23E-07	4.88	7.34E-09	4.92	9.71E-08	4.87
320 × 320	6.22E-10	4.94	7.12E-09	4.97	2.34E-10	4.97	3.11E-09	4.97
640 × 640	1.81E-11	5.10	2.24E-10	4.99	7.37E-12	4.99	9.77E-11	4.99

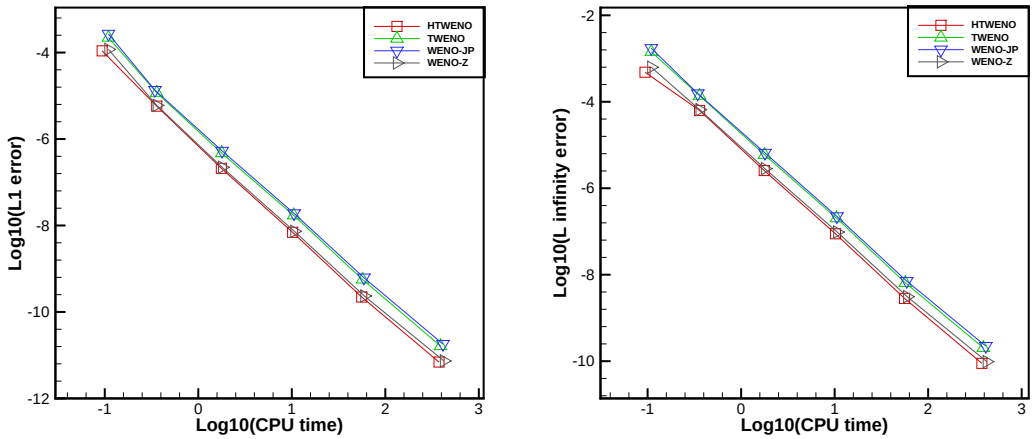

Figure 2: Example 3.2. Computing time and error.

merical accuracy orders, for four distinct finite difference WENO schemes. Fig. 2 clearly demonstrates that the HTWENO scheme continues to exhibit its characteristics of high computational efficiency and low truncation errors.

Example 3.3 (Linear Equation with Discontinue Initial Condition)**.** We test the simulation capability of the scheme for discontinuous problems starting with the linear equation

$$\psi_t + \psi_x = 0$$

with periodic boundary conditions and the initial condition

$$\psi(x,0) = \psi_0(x-0.5),$$

where

$$\psi_0(x) = -\left(\frac{\sqrt{3}}{2} + \frac{9}{2} + \frac{2\pi}{3}\right)(x+1) + \begin{cases} 2\cos\left(\frac{3\pi x^2}{2}\right) - \sqrt{3}, & x \in [-1,-1/3), \\ \frac{3}{2} + 3\cos(2\pi x), & x \in [-1/3,-0), \\ \frac{15}{2} - 3\cos(2\pi x), & x \in [0,1/3), \\ \frac{28+4\pi+\cos(3\pi x)}{3} + 6\pi x(x+1), & x \in [1/3,1]. \end{cases}$$

The grid points are set to 100. Fig. 3 shows numerical solutions obtained by four different WENO schemes at final times of 2 and 8, respectively. It can be observed that the HTWENO scheme yields the closest approximation to the exact solution, followed closely by the WENO-Z scheme in terms of numerical performance.

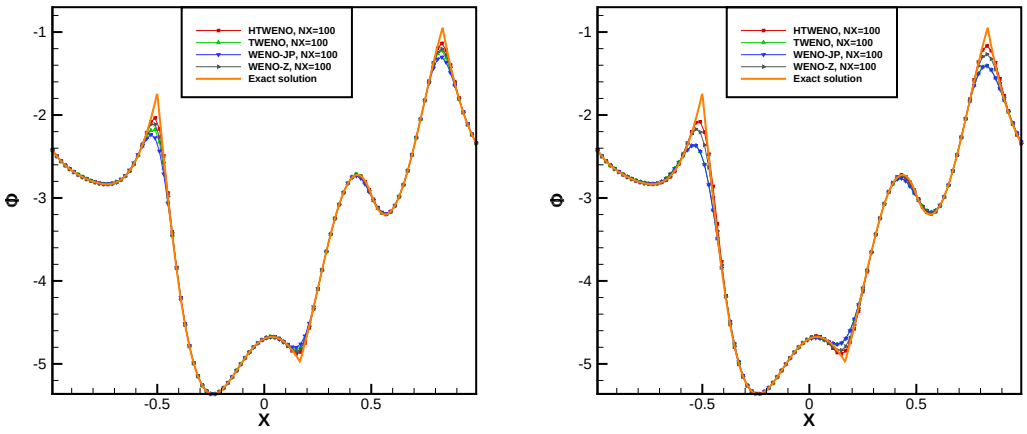

(a) T = 2 (b) T = 8

Figure 3: Example 3.3. Exact solution: solid line; HTWENO: squares; TWENO: upward triangles; WENO-JP: downward triangles; WENO-Z: rightward triangles.

Example 3.4 (One-Dimensional Nonlinear Burgers' Equation)**.** Next we evaluate the performance of the HTWENO scheme for the nonlinear equation

$$\psi_t + \frac{(\psi_x + 1)^2}{2} = 0,$$

subject to periodic boundary constraints and the initial profile

$$\psi_0(x) = -\cos(\pi x).$$

Based on the tests conducted in previous examples, we have found that, apart from the HTWENO scheme, the WENO-Z scheme exhibits the best numerical performance. Therefore, in subsequent examples, we will only compare it with the WENO-Z scheme. The numerical results of HTWENO and WENO-Z schemes are shown in Fig. 4 at $t = 3.5/\pi^2$

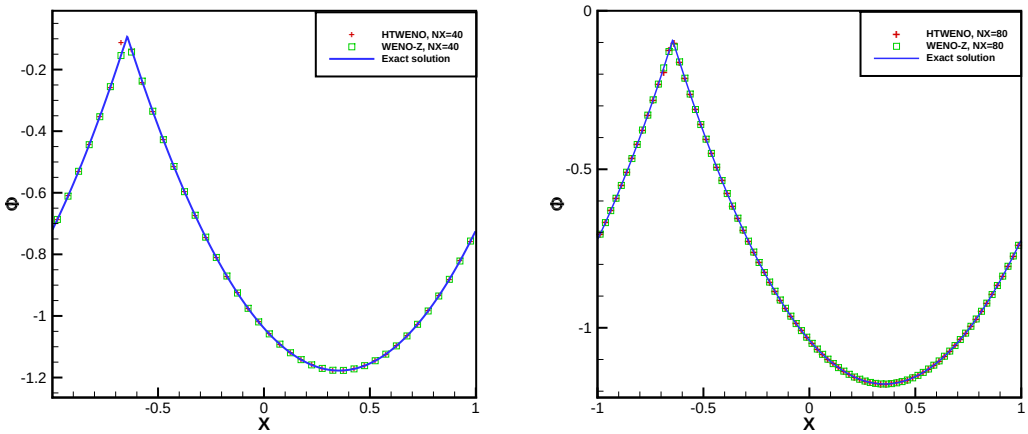

Figure 4: Example 3.4. Exact solution: solid line; HTWENO: crosses; WENO-Z: squares.

with different grids. At this specific moment, the solution exhibits certain discontinuities. Notably, the newly introduced finite difference HTWENO scheme demonstrates commendable performance for this particular test case.

Example 3.5 (A Nonlinear Equation Characterized by a Non-Convex Flux Function)**.** We conduct a study of a specific equation

$$\psi_t - \cos(\psi_x + 1) = 0,$$

subject to initial conditions $\psi_0(x) = -\cos(\pi x)$ and periodic boundary constraints. The simulation runs until $t = 1.5/\pi^2$. The shape of the solution at the final time is displayed in Fig. 5. Notably, the newly proposed finite difference HTWENO scheme exhibits excellent performance for this particular example.

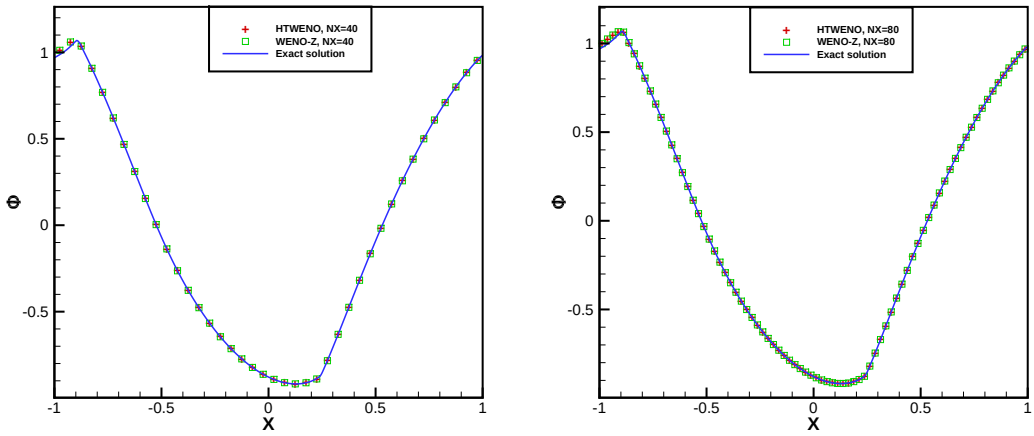

Figure 5: Example 3.5. Exact solution: solid line; HTWENO: crosses; WENO-Z: squares.

Example 3.6 (One-Dimensional Riemann Problem)**.** We delve into the 1D Riemann problem, formulated as

$$\psi_t + \frac{1}{4}\left(\psi_x^2 - 1\right)\left(\psi_x^2 - 4\right) = 0 \quad \text{for} \quad x \in (-1, 1),$$
$$\psi_0(x) = -2|x|.$$

This example presents a considerable hurdle, as numerous numerical approaches lacking adequate resolution struggle to attain a solution that aligns with the viscosity criteria. To validate our numerical approach, we present the results obtained at $t = 1$ using a grid of 80 points in Fig. 6. Remarkably, the newly devised finite difference HTWENO scheme demonstrates exceptional performance in tackling this intricate problem.

Example 3.7 (Two-Dimensional Burgers' Equation)**.** We investigate the characteristics of a 2D Burgers' equation (3.2), initiating with the initial state

$$\psi_0(x, y) = -\cos\left(\frac{\pi}{2}(x + y)\right).$$

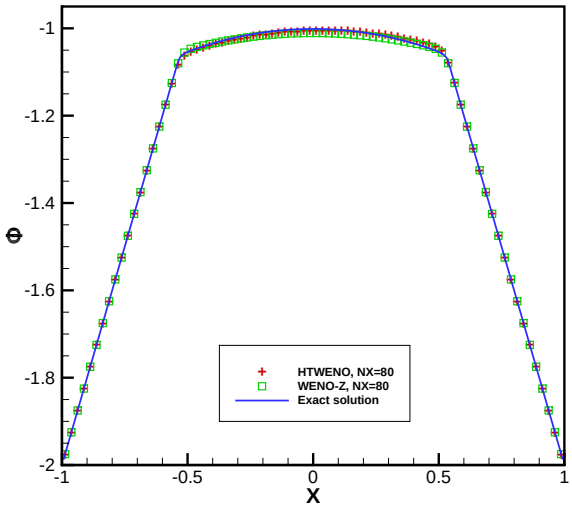

Figure 6: Example 3.6. Exact solution: solid line; HTWENO: crosses; WENO-Z: squares.

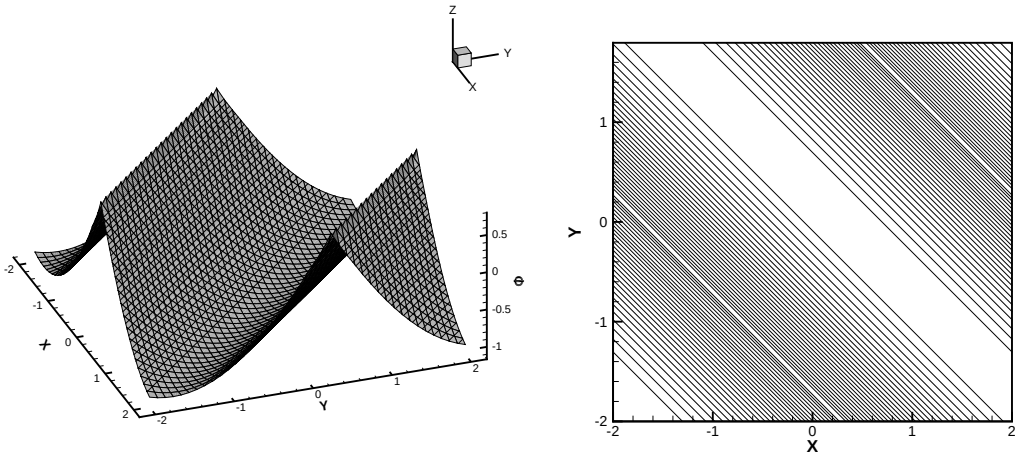

Figure 7: Example 3.7. Left: the surface of the solution. Right: contours of the solution.

Initially, the solution exhibits a smooth profile, making it an ideal candidate for accuracy testing at $t = 0.5/\pi^2$. As time progresses to $t = 1.5/\pi^2$, a notable discontinuity emerges in the derivative of the solution. To visualize this development, we present the numerical results obtained at $t = 1.5/\pi^2$ in Fig. 7, which clearly depicts the discontinuous behavior in the solution.

Example 3.8 (Two-Dimensional Riemann Problem)**.** We explore a particular mathematical model, characterized by a nonlinear partial differential equation, within a square region

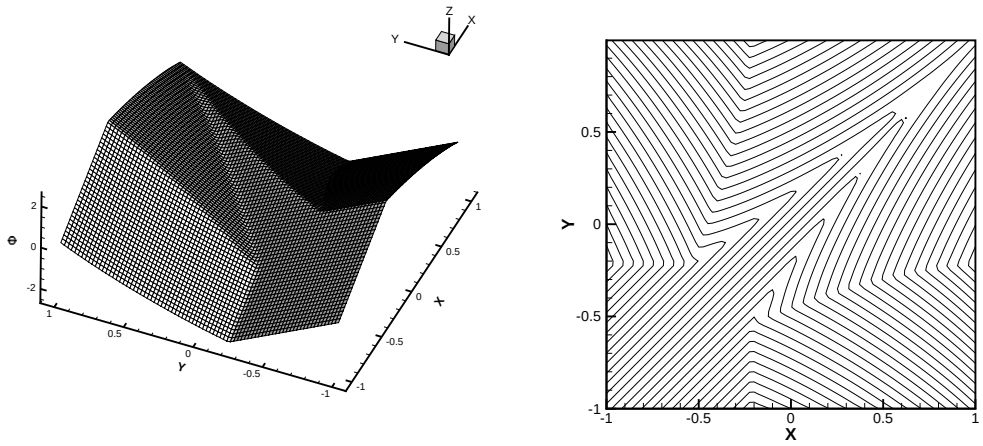

Figure 8: Example 3.8. Left: the surface of the solution. Right: contours of the solution.

defined by $-1 \le x, y \le 1$

$$\begin{aligned} &\psi_t + \sin(\psi_x + \psi_y) = 0 \quad \text{for } (x,y) \text{ in the domain,} \\ &\psi_0(x,y) = \pi(|y| - |x|) \quad \text{at the initial time.} \end{aligned}$$

This equation poses a significant challenge due to its complex behavior and the need for numerical methods to accurately capture its solution. In Fig. 8, we display the numerical results obtained using the HTWENO scheme at $t = 1$. This simulation yields high-resolution outcomes.

Example 3.9 (Two-Dimensional Optimal Control Problem)**.** We evaluate the equation

$$\begin{aligned} &\psi_t + \sin(y)\psi_x + \big(\sin(x) + \operatorname{sign}(\psi_y)\big)\psi_y \\ &\quad - \frac{1}{2}\sin^2(y) - \big(1 - \cos(x)\big) = 0, \quad -\pi \le x, y \le \pi, \\ &\psi_0(x,y) = 0, \end{aligned}$$

subject to periodic boundary conditions. This equation often arises in the context of optimal control theory. Utilizing the new finite difference HTWENO scheme, we plot the numerical solutions at $t = 1$ and depict the optimal control $\omega = \operatorname{sign}(\psi_y)$ in Fig. 9.

Example 3.10 (Eikonal Equation)**.** A mathematical model relevant to geometric optics, characterized by a nonlinear wavefront propagation equation, can be formulated as

$$\begin{aligned} &\psi_t + \sqrt{\psi_x^2 + \psi_y^2 + 1} = 0, \quad (x,y) \in [0,1] \times [0,1], \\ &\psi_0(x,y) = \frac{1}{4}\big(\cos(2\pi x) - 1\big)\big(\cos(2\pi y) - 1\big) - 1. \end{aligned}$$

Fig. 10 demonstrates numerical results obtained by novel finite difference HTWENO scheme at $t = 0.6$. These results demonstrate a high degree of resolution for the numerical simulation in question.

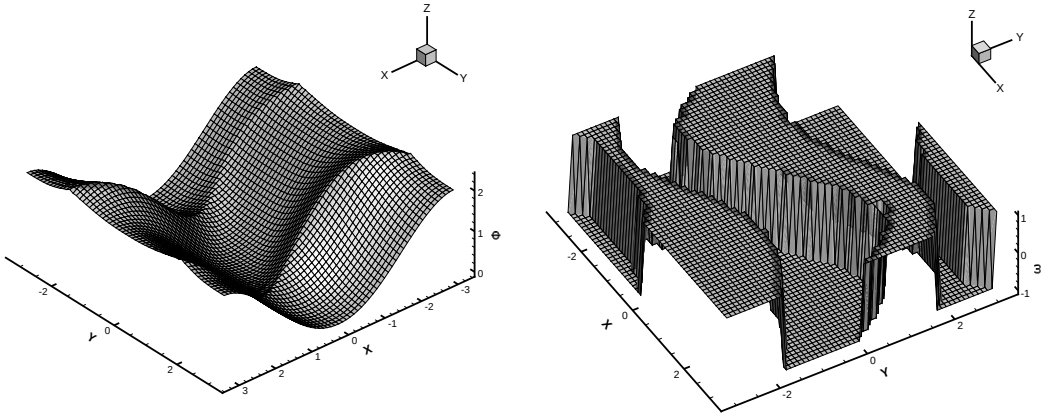

Figure 9: Example 3.9. Left: the surface of the solution. Right: the optimal control.

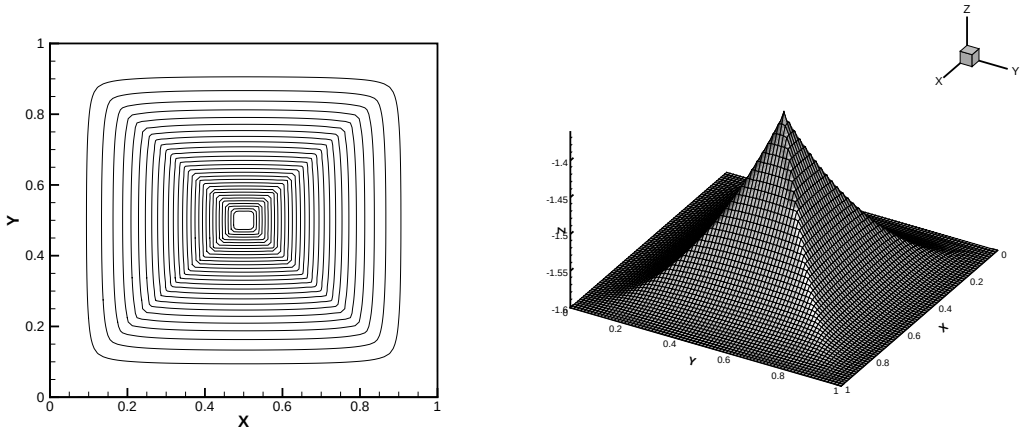

Figure 10: Example 3.10. Left: contours of the solution. Right: the surface of the solution.

Example 3.11 (A Problem Involving the Progression of a Surface)**.** The advancement of a surface described in [31], involves the equation

$$\psi_t - (1-\varepsilon T)\sqrt{\psi_x^2+\psi_y^2+1} = 0, \quad (x,y)\in[0,1]\times[0,1],$$
$$\psi_0(x,y) = 1 - \frac{1}{4}\big(\cos(2\pi x)-1\big)\big(\cos(2\pi y)-1\big),$$

where T denotes the mean curvature — i.e.

$$T = -\frac{\psi_{xx}(1+\psi_y^2) - 2\psi_{xy}\psi_x\psi_y + \psi_{yy}(1+\psi_x^2)}{(1+\psi_x^2+\psi_y^2)^{3/2}},$$

and ε represents a minute constant and boundary conditions are periodic in both directions. Fig. 11 displays the numerical results obtained using the new finite difference HTWENO scheme at various time, comparing cases with $\varepsilon = 0$ (representing pure convection) and $\varepsilon = 0.1$.

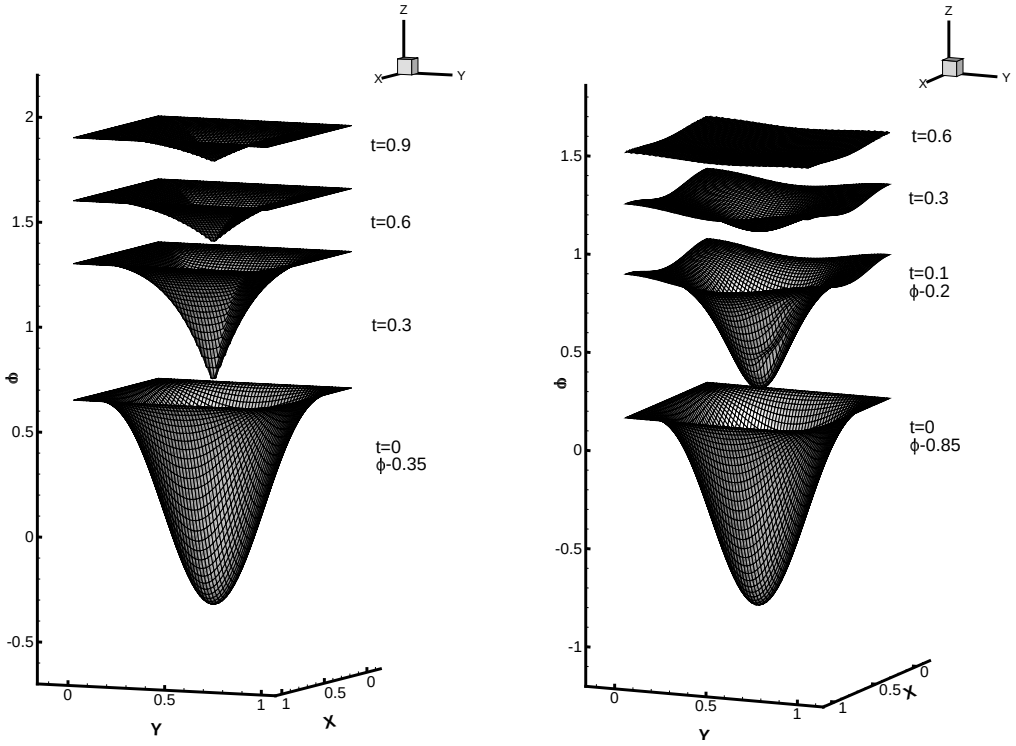

Figure 11: Example 3.11. Left: $\varepsilon = 0$. Right: $\varepsilon = 0.1$. 60×60 points.

4. Concluding Remarks

We propose a hybrid TWENO scheme for solving HJ equations on structured grids. This scheme innovatively hybridizes it with three linear schemes to achieve higher resolution near discontinuities. The main advantages of this scheme are its robustness and computational efficiency compared to the traditional WENO-JP scheme [20]. The hybrid approach also demonstrates excellent scalability and can be easily combined with other schemes such as the US-WENO and MR-WENO schemes. In future work, we plan to combine this method with radial basis function (RBF) polynomials to develop a higher-order WENO scheme with enhanced robustness and higher resolution.

Acknowledgments

The research is partly supported by the NSFC (Grant No. 12501548), by the Science Challenge Project (Grant No. TZZT20240303), by the Science and Technology Key Project of Henan Province of China (Grant Nos. 242102110145, 252102220057), by the Key Scientific Research Project of Henan Higher Education Institutions of China (Grant No. 26A110011), and by the Natural Science Foundation of Henan Province (Grant No. 252300420333).

References

[1] S. Augoula and R. Abgrall, *High order numerical discretization for Hamilton-Jacobi equations on triangular meshes*, J. Sci. Comput. **15**, 198–229 (2000).

[2] D.S. Balsara, T. Rumpf, M. Dumbser and C.D. Munz, *Efficient, high accuracy ADER-WENO schemes for hydrodynamics and divergence-free magnetohydrodynamics*, J. Comput. Phys. **228**, 2480–2516 (2009).

[3] W. Baron, *Zur trigonometrischen interpolation*, Computing **16**, 319–328 (1976).

[4] T.J. Barth and J.A. Sethian, *Numerical schemes for the Hamilton-Jacobi and level set equations on triangulated domains*, J. Comput. Phys. **145**, 1–40 (1998).

[5] S. Bryson and D. Levy, *High-order central WENO schemes for multidimensional Hamilton-Jacobi equations*, SIAM J. Numer. Anal. **41**, 1339–1369 (2003).

[6] S. Bryson and D. Levy, *Mapped WENO and weighted power ENO reconstructions in semi-discrete central schemes for Hamilton-Jacobi equations*, Appl. Numer. Math. **56**, 1211–1224 (2006).

[7] M. Castro, B. Costa and W.S. Don, *High order weighted essentially non-oscillatory WENO-Z schemes for hyperbolic conservation laws*, J. Comput. Phys. **5(230)**, 1766–1792 (2011).

[8] A. Chertock, S. Chu and A. Kurganov, *Adaptive high-order A-WENO schemes based on a new local smoothness indicator*, East Asian J. Appl. Math. **13**, 576–609 (2023).

[9] S. Christofi, *The study of building blocks for essentially non-oscillatory (ENO) schemes,* PhD. Thesis, Brown University, 1996.

[10] B. Cockburn and C.-W. Shu, *TVB Runge-Kutta local projection discontinuous Galerkin finite-element method for conservation laws II: General framework*, Math. Comp. **52**, 411–435 (1989).

[11] M.G. Crandall, L.C. Evans and P.L. Lions, *Some properties of viscosity solutions of Hamilton-Jacobi equations*, Trans. Amer. Math. Soc. **282**, 487–502 (1984).

[12] M.G. Crandall, H. Ishii and P.L. Lions, *Users guide to viscosity solutions of second order partial equations*, Bull. Amer. Math. Soc. **27**, 1–67 (1992).

[13] M.G. Crandall and P.L. Lions, *Viscosity solutions of Hamilton-Jacobi equations*, Trans. Amer. Math. Soc. **277**, 1–42 (1983).

[14] M.G. Crandall and P.L. Lions, *Two approximations of solutions of Hamilton-Jacobi equations*, Math. Comput. **43**, 1–19 (1984).

[15] P. Deng, G. Peng, X. Feng, D. Luo and Y. Chen, *A finite volume simple WENO scheme for convection-diffusion equations*, Numer. Math. Theory Methods Appl. **17**, 882–903 (2024).

[16] Z. Gao, S. Guo, B. Wang and Y. Gu, *High order bound- and positivity-preserving finite difference affine-invariant AWENO scheme for the five-equation model of two-medium flows*, Commun. Comput. Phys. **36**, 781–820 (2024).

[17] A. Harten, B. Engquist, S. Osher and S. Chakravarthy, *Uniformly high-order accurate non-oscillatory schemes III*, J. Comput. Phys. **71**, 231–303 (1987).

[18] A. Harten and S. Osher, *Uniformly high-order accurate non-oscillatory schemes I*, SIAM J. Numer. Anal. **24(2)**, 279–309 (1987).

[19] C. Hu and C.-W. Shu, *A discontinuous Galerkin finite element method for Hamilton-Jacobi equations*, SIAM J. Sci. Comput. **21**, 666–690 (1999).

[20] G.-S. Jiang and D. Peng, *Weighted ENO schemes for Hamilton-Jacobi equations*, SIAM J. Sci. Comput. **21**, 2126–2143 (2000).

[21] G.-S. Jiang and C.-W. Shu, *Efficient implementation of weighted ENO schemes*, J. Comput. Phys. **126**, 202–228 (1996).

[22] L. Krivodonova, J. Xin, J.F. Remacle, N. Chevaugeon and J. Flaherty, *Shock detection and limiting with discontinuous Galerkin methods for hyperbolic conservation laws*, Appl. Numer. Math. **48**, 323–338 (2004).

[23] F. Lafon and S. Osher, *High order two dimensional nonoscillatory methods for solving Hamilton-Jacobi scalar equations*, J. Comput. Phys. **123**, 235–253 (1996).
[24] O. Lepsky, C. Hu and C.-W. Shu, *Analysis of the discontinuous Galerkin method for Hamilton-Jacobi equations*, Appl. Numer. Math. **33**, 423–434 (2000).
[25] G. Li, C. Lu and J.-X. Qiu, *Hybrid well-balanced WENO schemes with different indicators for shallow water equations*, J. Sci. Comput. **51**, 527–559 (2012).
[26] G. Li and J.-X. Qiu, *Hybrid weighted essentially non-oscillatory schemes with different indicators*, J. Comput. Phys. **229**, 8105–8129 (2010).
[27] G. Li and J.-X. Qiu, *Hybrid WENO schemes with different indicators on curvilinear grids*, Adv. Comput. Math. **40**, 747–772 (2017).
[28] J. Li, C.-W. Shu and J. Qiu, *Derivative-based finite-volume MR-HWENO scheme for steady-state problems*, Commun. Comput. Phys. **36**, 877–907 (2024).
[29] X.-D. Liu, S. Osher and T. Chan, *Weighted essentially non-oscillatory schemes*, J. Comput. Phys. **115**, 200–212 (1994).
[30] J. Mu, C. Zhuo, Q. Zhang, S. Liu and C. Zhong, *An efficient high-order gas-kinetic scheme with hybrid WENO-AO method for the Euler and Navier-Stokes solutions*, Commun. Comput. Phys. **35**, 662–692 (2024).
[31] S. Osher and J. Sethian, *Fronts propagating with curvature dependent speed: Algorithms based on Hamilton-Jacobi formulations*, J. Comput. Phys. **79**, 12–49 (1988).
[32] S. Osher and C.-W. Shu, *High-order essentially non-oscillatory schemes for Hamilton-Jacobi equations*, J. Comput. Phys. **28**, 907–922 (1991).
[33] J. Qiu and C.-W. Shu, *Hermite WENO schemes for Hamilton-Jacobi equations*, J. Comput. Phys. **204**, 82–99 (2005).
[34] C.-W. Shu, *Numerical experiments on the accuracy of ENO and modified ENO schemes*, J. Sci. Comput. **5**, 127–150 (1990).
[35] C.-W. Shu and S. Osher, *Efficient implementation of essentially non-oscillatory shock capturing schemes*, J. Comput. Phys. **77**, 439–471 (1988).
[36] C.-W. Shu and S. Osher, *Efficient implementation of essentially non-oscillatory shock capturing schemes II*, J. Comput. Phys. **83**, 32–78 (1989).
[37] Y.M. Wang and J. Zhu, *A new type of increasingly high-order multi-resolution trigonometric WENO schemes for hyperbolic conservation laws and highly oscillatory problems*, Comput. Fluids **200**, Paper No. 104448 (2020).
[38] Y.M. Wang, J. Zhu and L. Xiong, *A new fifth-order trigonometric WENO scheme for hyperbolic conservation laws and highly oscillatory problems*, Adv. Appl. Math. Mech. **11(5)**, 1114–1135 (2019).
[39] Y. Zhang and J. Zhu, *New mapped unequal-sized trigonometric WENO scheme for hyperbolic conservation laws*, Comput. Fluids **245**, Paper No. 105585 (2020).
[40] J. Zhu and J.X. Qiu, *Trigonometric WENO shemes for hyperbolic conservation laws and highly oscillatory problems*, Commun. Comput. Phys. **8**, 1242–1263 (2010).
[41] J. Zhu and J.X. Qiu, *A new fifth order finite difference WENO scheme for Hamilton-Jacobi equations*, Numer. Methods Partial Differential Equations **33(4)**, 1095–1113 (2016).
[42] J. Zhu and J.-X. Qiu, *A new type of modified WENO schemes for solving hyperbolic conservation laws*, SIAM J. Sci. Comput. **2**, A1089–A1113 (2017).